Journal of Alloys and Compounds 504 (2010) 435–439

Contents lists available at ScienceDirect

Journal of Alloys and Compounds

journal homepage: www.elsevier.com/locate/jallcom

Electrical and magnetic properties of NiCuZn–$CaCu_3Ti_4O_{12}$ composites doped with Bi_2O_3

Ying He[a,*], Huaiwu Zhang[a], Yunyan Wang[a], Weiwei Ling[a], Chunhong Mu[a], Feiming Bai[a], Peng Liu[b]

[a] The Key Laboratory of Electronic Thin Film and Integrated Devices, University of Electronic Science and Technology of China, Chengdu 610054, PR China
[b] College of Physics and Information Technology, Shaanxi Normal University, Xi'an 710062, PR China

ARTICLE INFO

Article history:
Received 3 September 2009
Received in revised form 29 May 2010
Accepted 1 June 2010
Available online 11 June 2010

Keywords:
Ceramics
Composite
Magnetic properties
Dielectric properties

ABSTRACT

Bi_2O_3 was used to promote grain growth and to improve magnetic and dielectric properties of NiCuZn ferrite–$CaCu_3Ti_4O_{12}$ composites during sintering. For a sintering temperature lower than 950 °C, the static permeability of the composites increases with the Bi_2O_3 content. Comparing with the composites without Bi_2O_3, the composite with Bi_2O_3 has a higher real permittivity and a lower loss tangent. With further increasing sintering temperature, it was found that the sample with 1 wt% Bi_2O_3 sintered at 1050 °C has the maximum static permeability, however, this was accompanied by an extremely high dielectric loss tangent. These results were analyzed in terms of the microstructures of the composites by scanning electron microscopy.

1. Introduction

Electronic–magnetic composite materials which possess both capacitive and inductive properties have attracted much attention due to their potential applications in many electronic devices, such as electromagnetic interference filters and integrated chip inductors and capacitors [1,2]. Many material systems, such as NiCuZn ferrite–(Ba, Sr)TiO_3, NiCuZn ferrite–PNNT and NiCuZn ferrite–Pb(Zr, Ti)O_3 have been prepared in the last few years [3–8]. $CaCu_3Ti_4O_{12}$ (CCTO), a typical giant dielectric material, has recently attracted many attentions due to its unusually dielectric properties of high and relatively temperature-independent permittivity value of >10,000 over a wide temperature range ~100–600 K [9,10]. The effects of CCTO on dielectric and magnetic properties of the NiCuZn ferrite–CCTO composite materials have been investigated in our previous work as the dielectric component [11], and the results showed that the dielectric constant ε' of the composites measured at 1 MHz increases gradually with the increasing of CCTO contents, while the real part permeability μ' at 1 MHz decreases significantly. By a comprehensive evaluation of both magnetic and dielectric properties, we choose the composition of 85 wt% NiCuZn + 15 wt% CCTO in here.

However, to realize extremely integrated and miniaturized RF modules, the sintering temperature (<961 °C) of materials has to be decreased to meet the requirement of low temperature co-fired ceramic (LTCC) technology [12]. There are several groups [13–15] using wet chemistry methods or mechanical alloying techniques to synthesize CCTO at lower temperatures, but these methods are relatively complex and extremely difficult to realize industrialization. On the other hand, Bi_2O_3, as the most effective sintering aid, is usually introduced into NiCuZn ferrite to promote the low-temperature sintering [16]. Thus, in this paper, Bi_2O_3 is considered as an alternative additive for improving the sintering behavior and its effect on electrical and magnetic properties of NiCuZn ferrite–CCTO composite materials are studied.

2. Experimental details

The NiCuZn ferrite (Ni:Cu:Zn:Fe = 0.21:0.13:0.66:2.00) was prepared through solid-state reaction using analytical grade NiO, CuO, ZnO, and Fe_2O_3 as raw materials. These basic oxides were mixed and wet milled for 12 h and pre-sintered at 900 °C for 2 h. Single-phase powders of $CaCu_3Ti_4O_{12}$ were prepared by the mixed oxide route from appropriate amounts of analytical grade $CaCO_3$, TiO_2, CuO and pre-sintered at 1000 °C for 10 h. Thereafter, these two powders were utilized to prepare the ceramic composites with the nominal composition of 85 wt% NiCuZn + 15 wt% CCTO. The powders were ground with x wt% Bi_2O_3 (x = 0, 1, 2, 3) in planetary mill for 12 h with water media. Then, the composite mixtures were dried, mixed with 10 wt% poly(ethylene glycol) binder, and pressed at 5 MPa to the shape of toroids (Ø18 mm × 8 mm) and pellets (Ø18 mm) with 2–3 mm thickness. The toroids and pellets were final sintered at temperatures ranging from 900 to 1050 °C for 2 h in air to yield the final specimens and the lattice parameters of ferrite in the composites were obtained by the software of Jade 6.5 (Rigaku, Japan), in which you can separate the peaks belonging to the phase you want to perform the cell refinement. The phase formation was examined by an X-ray diffractometer (D/max-2550/PC, Rigaku, Japan) with Cu Kα radiation. The microstructures were observed by a scanning electron microscope (JSM-6490, JEOL, Japan) equipped with an energy dispersive spectrometer. The complex permeability and permittivity were measured by a precision LCR meter (Agilent 4284A, USA) in the frequency range of 40 Hz to 1 MHz

* Corresponding author.
E-mail address: yhe229@gmail.com (Y. He).

0925-8388/$ – see front matter © 2010 Elsevier B.V. All rights reserved.
doi:10.1016/j.jallcom.2010.06.001

and an impedance analyzer (HP4291B, USA) in the frequency range of 1 MHz to 1.8 GHz.

3. Results and discussion

3.1. Phase identification and microstructure

The diffraction patterns of the composites were identified to be mainly spinel ferrite structure, and the dielectric phase is detected as a second phase. No Bi_2O_3 phase was observed in our XRD measurement (not shown here), which is probably due to the very low Bi_2O_3 content. A comparison between the XRD patterns of composites reveals that no obvious peak shifting of ferrite phase is observed as Bi_2O_3 increases from 0 to 3 wt%. For example, the corresponding lattice constant of ferrite in the composites sintered at 1050 °C are 8.4125, 8.4247, 8.4180, and 8.4283 Å, respectively.

The densities of the composites sintered at different temperature are shown in Fig. 1. All of the samples achieve >95% of the theoretical density (5.26 g/cm^3) except for the sample without Bi_2O_3 sintered at 900 °C. Owing to the very low addition of Bi_2O_3 ($\leq$3 wt%) here, its role has not been specifically considered in estimating the theoretical density of the composites.

The cross-sectional SEM photographs of the composites sintered at 950 °C are shown in Fig. 2. With increasing the content of Bi_2O_3, it can be seen that the grain size obviously increases and the microstructure shows a smaller portion of porosity. This clearly indicates that the addition of Bi_2O_3 significantly enhances the grain growth rate and the densification of the samples, which can be attributed to the formation of a liquid phase during the sintering process [17].

To investigate the effects of Bi_2O_3, we have furthered raised the sintering temperature to 1050 °C. Fig. 3(a)–(c) shows the typical cross-sectional SEM photographs of the composites. Apparently,

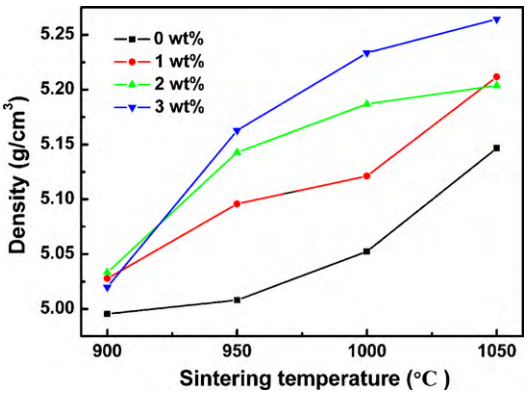

Fig. 1. Variation of sample density with sintering temperature.

the sample sintered at 1050 °C has a larger grain size than that sintered at 950 °C. It can be seen that the sample without Bi_2O_3 still shows a microstructure with many point contacts among grains. As the content of Bi_2O_3 is increased to 1 wt%, the sample becomes denser, and less point contacts are observable. However, a higher amount of Bi_2O_3 (3 wt%) causes anomalous grain growth and many closed pores in grains, as shown in Fig. 3(c). In addition, thick boundary layers can be found between neighboring large grains. According to EDS analysis of the composite with 3 wt% Bi_2O_3, the quantitative ratios of different cations, Ca:Ti:Zn:Fe:Bi, of the grain (labelled G in Fig. 3c) and grain boundary (labelled GB in Fig. 3c) are 1.05:2.92:10.24:22.48:0 and 1.73:5.03:7.96:23.92:3.03, respectively. The result reveals that the grain boundary region is rich in Bi. Moreover, the quantitative ratio of (Ca + Ti) to (Zn + Fe) in grain boundary region is more than 2 times higher than that in the grain

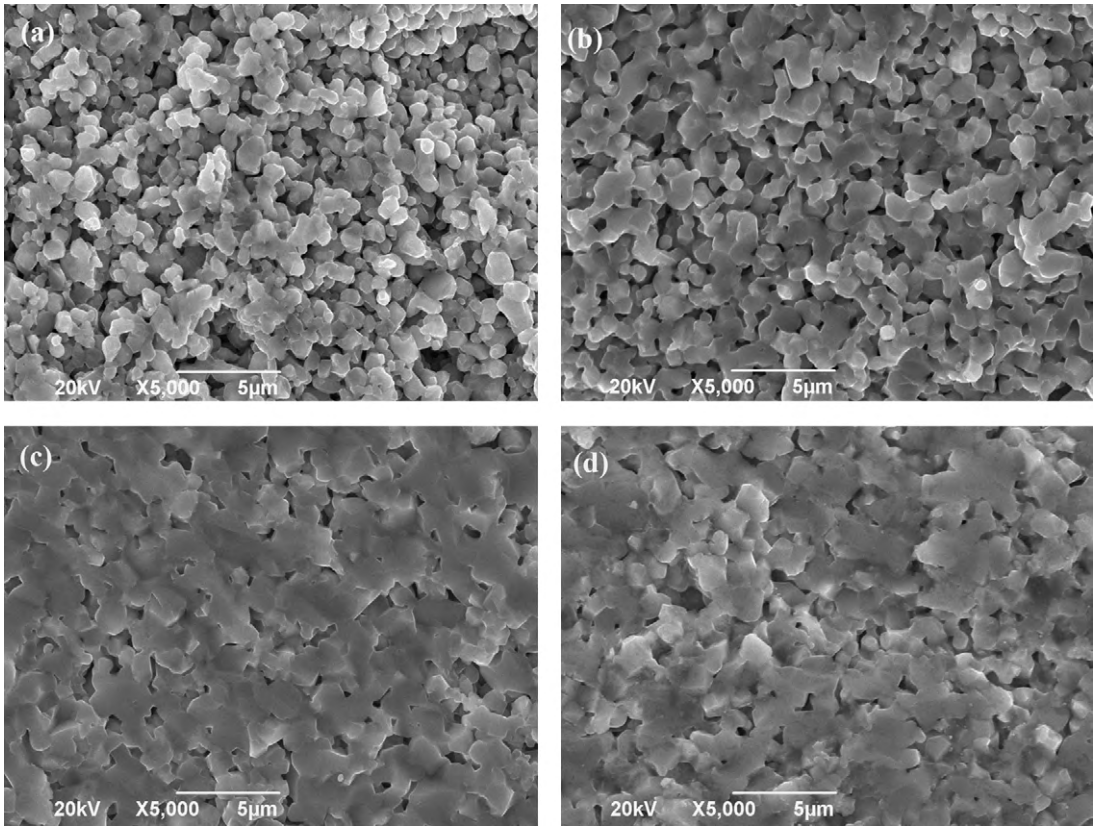

Fig. 2. SEM micrographs of the composites sintered at 950 °C with (a) 0 wt%, (b) 1 wt%, (c) 2 wt%, and (d) 3 wt% Bi_2O_3.

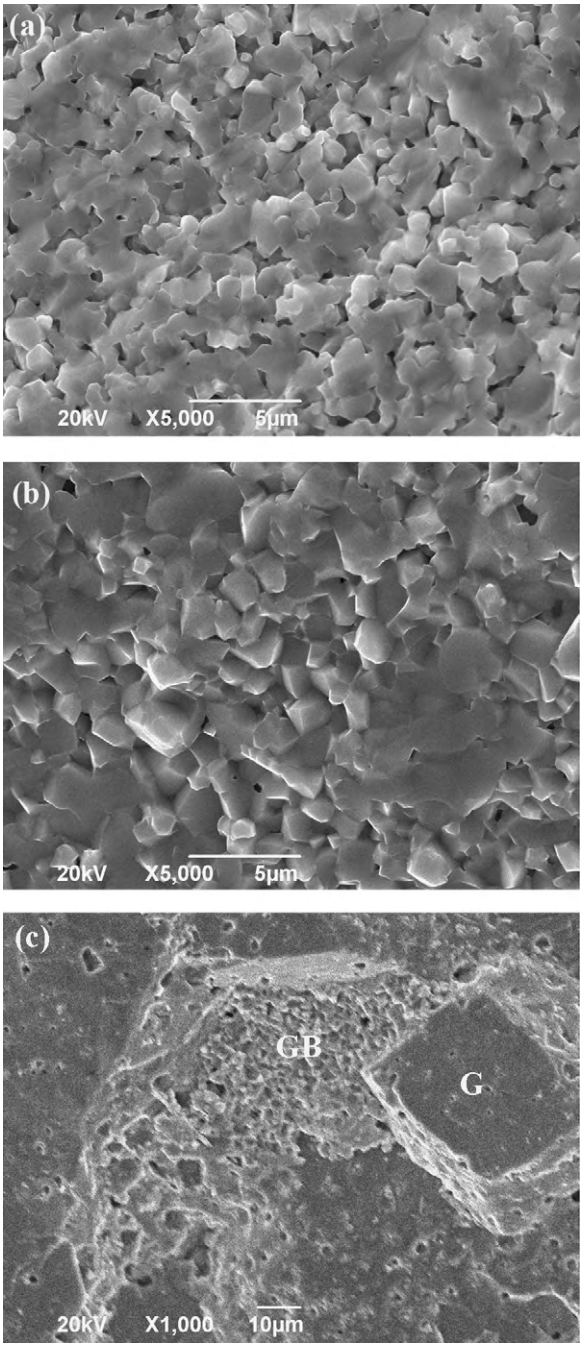

Fig. 3. SEM micrographs of the composites sintered at 1050 °C with (a) 0 wt%, (b) 1 wt%, (c) 3 wt% Bi_2O_3. Labels G and GB in (c) denote the grain and grain boundary, respectively.

region. This result indicates that the presence of CCTO is more like at the grain boundaries of the ferrite.

3.2. Magnetic properties

Fig. 4 is the frequency dependence of the complex permeability for the composites sintered at different temperatures. These composites exhibit the plateaus in the real permeability μ' below a certain frequency, above which μ' rapid drops. The resonance frequency of the dispersion is about 10^7 to 10^8 Hz, which corresponds to the peak in the imaginary permeability μ''. Variations of permeability and resonance frequency follow the Snoek's law [18], and the peak shifts to a lower frequency side as the real permeability increases.

The static permeability μ_0 of the composites with and without Bi_2O_3 is further shown in Fig. 5 as a function of sintering temperature. Here, the real permeability at 1 MHz is used as the static permeability because it remains almost constant below 1 MHz. It can be seen that the static permeability of all the composites increases with the increase of sintering temperature, except for the composite with 3 wt% Bi_2O_3. As the sintering temperature is ≤950 °C, μ_0 increases with the Bi_2O_3 content. For the sintering temperature of 1000 °C, the static permeability of the 2 wt% sample is almost same as that of the 3 wt% sample. At 1050 °C, a maximum static permeability is obtained in the sample with 1 wt% Bi_2O_3 and the static permeability gradually decreases with further increasing the Bi_2O_3 content.

The magnetic permeability of polycrystalline ferrites strongly depends on the sintering density [16] and the grain size [19]. When the sintering density and the grain size increase, the permeability increases. On the other hand, the changes of the grain boundary constitution might have an essential influence on its magnetic permeability. In general, the foreign ions (additives or impurities) may affect grain boundaries by inducing micro-stress on the grain boundary and by the formation of a nonmagnetic grain boundary [17]. From the above considerations one can conclude that, as the sintering temperature is ≤950 °C, the increasing trend of μ_0 for the samples with Bi_2O_3 is dominantly controlled by the grain size and the sintering density. When the sintering temperature increases to 1050 °C, the factors affecting the static permeability become more complicated. For the sample with 3 wt% Bi_2O_3, in one hand, the increase in sintering density and grain size may enhance the static permeability; on the other hand, the closed pores in grains could pin domain wall motion [19], and the thick grain boundaries [17] also reduce the static permeability. Furthermore, for our composite materials, the large static permeability is mainly contributed by NiCuZn ferrites. The increase of Bi_2O_3 content enhances the total sintering density of composites, while it difficult to say whether the density of ferrites in the composites also increases. Consequently, a maximum value of static permeability occurs at the sample with 1 wt% Bi_2O_3 at 1050 °C.

According to the magnetic circuit model [20,21], the static permeability μ_0 is given by

$$\mu_0 = \frac{\mu_i(1+\delta/D)}{1+\mu_i(\delta/D)}, \tag{1}$$

where μ_i is the intrinsic static permeability of materials without any defects, and D and δ are the average grain size and thickness of the grain boundaries. As it is difficult to measure D and δ directly, the ratio δ/D is usually calculated approximately from the measured density (ρ_d) based on the following formula [22]

$$\frac{\delta}{D} = \left(\frac{\rho_{d,i}}{\rho_d}\right)^{1/3} - 1, \tag{2}$$

where $\rho_{d,i}$ is the theoretical density of the materials. Fig. 6 shows the variation of static permeability with δ/D for the composites sintered at different temperatures. On the basis of Eq. (1), a fitting calculation for the static permeability with δ/D is carried out and the intrinsic static permeability μ_i with the value of 394 is obtained. The value of the intrinsic static permeability is nearly double of the maximum static permeability of the composites, which is in agreement with the result reported in the literature [23]. It is seen that the static permeability of the composites is closed to the fitting curve. This means that the magnetic circuit model can be used to explain the present experimental results and it may be give valuable prediction for composite material design.

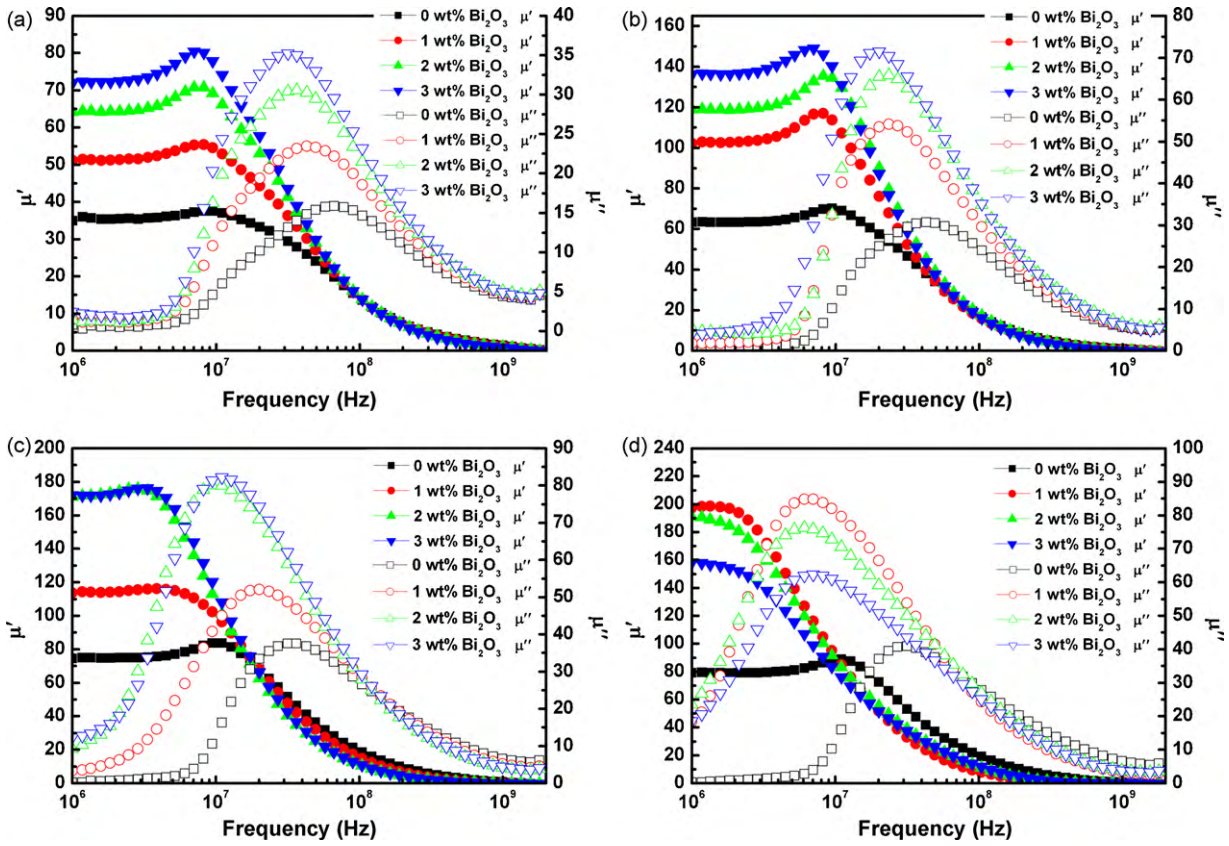

Fig. 4. Frequency dependence of complex permeability for the composites with different Bi_2O_3 contents sintered at (a) 900 °C, (b) 950 °C, (c) 1000 °C, and (d) 1050 °C.

3.3. Dielectric properties

Fig. 7 shows the frequency dependence of complex permittivity for the composites sintered at different temperatures. It can be seen that the real permittivity ε' increases gradually with increasing sintering temperature. However, the high ε' is accompanied by an extremely high dielectric loss tangent $\tan\delta$. At a given sintering temperature, these curves for the composites with Bi_2O_3 can be classified into two types. One is represented by those shown in Fig. 7(a) and (b), where both the real permittivity ε' and the dielectric loss tangent $\tan\delta$ are almost independent of frequency. Comparing with the composites without Bi_2O_3, the composite with Bi_2O_3 has a higher ε' and a lower loss tangent. The other type belongs to high loss composites, which are characterized by frequency dependent real permittivity and dielectric loss tangent, especially at low frequency (<10 MHz), as shown in Fig. 7(c) and (d).

The mechanism of the polarization process in ferrites is similar to that of the conduction process. By the electronic exchange $Fe^{2+} \leftrightarrow Fe^{3+}$, one obtains local displacements of electrons in the direction of the applied electrical field. These displacements determine the polarization of the ferrite [24]. However, polarization, which often occurs in the heterogeneous system where the conductivities of two components are different, may still arise from the interface between grains and grain boundaries, and causes the dispersion at 10^3 to 10^4 Hz, but it can extend to a high frequency of less than 100 MHz [25,26]. Therefore, the independent real permittivity shown in Fig. 7(a) and (b) possibly results from the incomplete formation of the barrier layer capacitance structure at low sin-

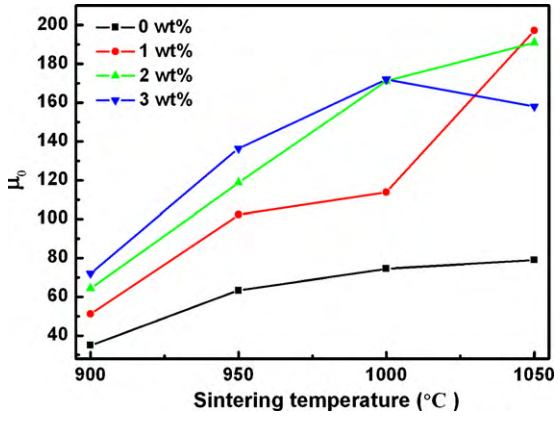

Fig. 5. Static permeability of the composites as a function of sintering temperature.

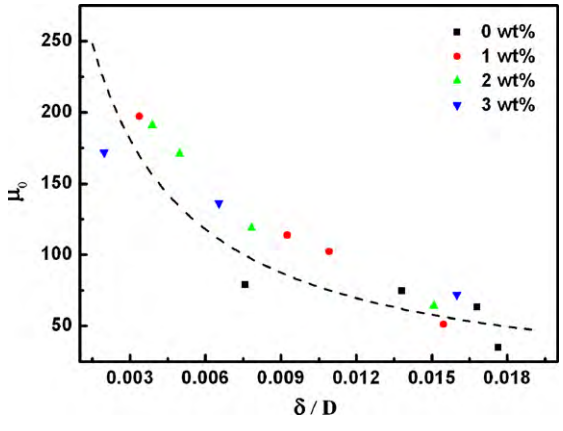

Fig. 6. Variation of static permeability with δ/D for the composites. The dashed line is the fitting curve.

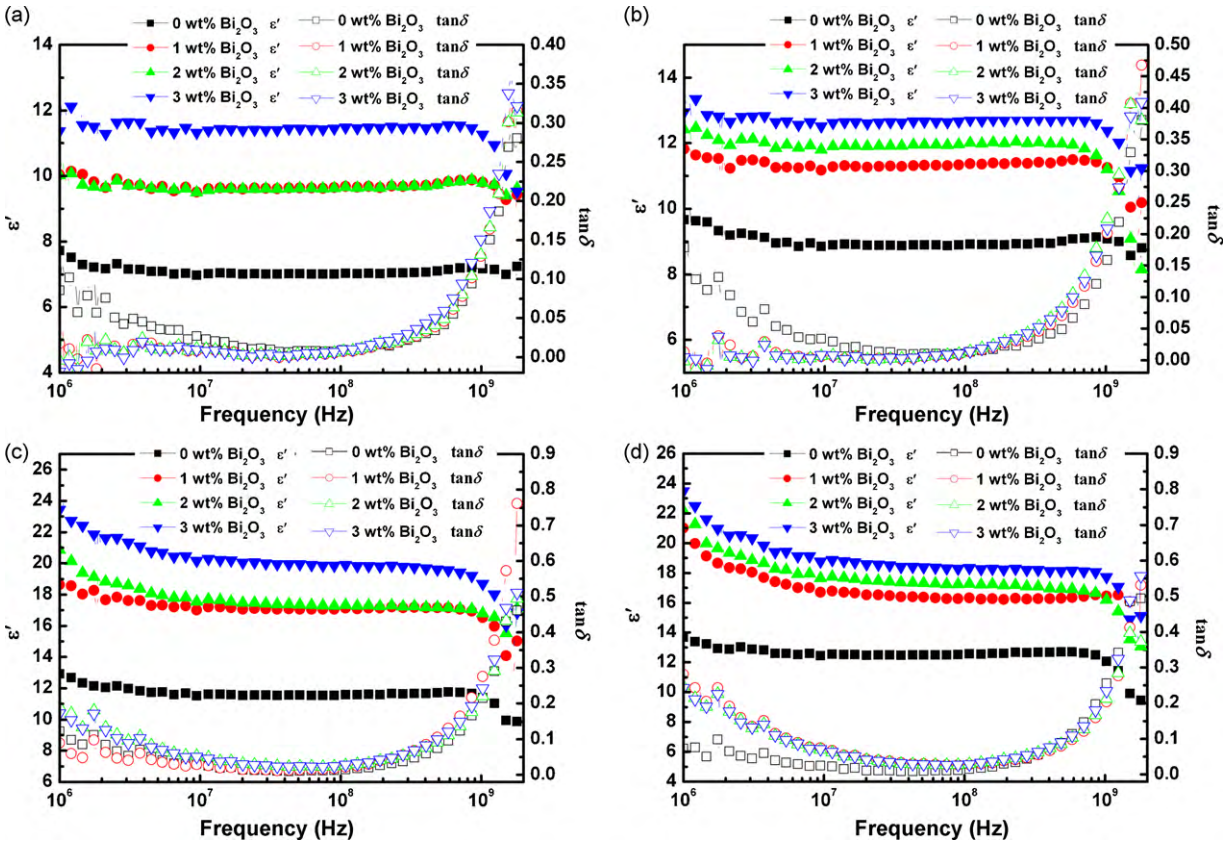

Fig. 7. Frequency dependence of complex permittivity for the composites with different Bi_2O_3 sintered at (a) 900 °C, (b) 950 °C, (c) 1000 °C, and (d) 1050 °C.

tering temperature, and, a higher loss tangent of the composites without Bi_2O_3 is caused by the conduction loss due to their porous microstructure [25].

4. Conclusions

The effects of Bi_2O_3 and sintering temperature on the microstructure, magnetic and dielectric properties of the NiCuZn ferrite–$CaCu_3Ti_4O_{12}$ composites have been investigated. SEM results show that the addition of Bi_2O_3 significantly enhances the grain growth rate and has a noticeable influence on the microstructure development of composites. The static permeability of the samples at low sintering temperature (≤950 °C) increases with the Bi_2O_3 content, which can be dominating attributed to the increase of grain size. At high sintering temperatures, the decrease of the static permeability of the samples with Bi_2O_3 (>1 wt%) can be attributed to either the closed pores in grains or the thick grain boundaries. The magnetic properties of the samples can be well explained by the magnetic circuit model. Moreover, the addition of Bi_2O_3 has a significant effect on decreasing dielectric loss of the samples sintered at low temperature (≤950 °C), which can be explained in terms of the microstructure with a smaller portion of porosity, together with the incomplete formation of the barrier layer capacitance structure.

Acknowledgements

This work is partly supported by the National Basic Research Program of China (973) under Grant No. 2007CB310407, Foundation for Innovative Research Groups of the NSFC under Grant No. 60721001, the International S&T Cooperation Program of China under Grant No. 2006DFA53410 and 2007DFR10250.

References

[1] X.W. Qi, J. Zhou, B.R. Li, Y.C. Zhang, Z.X. Yue, Z.L. Gui, L.T. Li, J. Am. Ceram. Soc. 87 (2004) 1848–1852.
[2] Y. Bai, J. Zhou, Z.L. Gui, L.T. Li, L.J. Qiao, J. Appl. Phys. 101 (2007) 083907-1–083907-6.
[3] H.W. Zhang, H. Zhong, B.Y. Liu, Y.L. Jing, Y.Y. Liu, IEEE Trans. Magn. 41 (2005) 3454–3456.
[4] X.W. Qi, J. Zhou, Z.X. Yue, Z.L. Gui, L.T. Li, S. Buddhudu, Adv. Funct. Mater. 14 (2004) 920–926.
[5] L.N. Su, P. Liu, Y. He, J.P. Zhou, L. Cao, C. Liu, H.W. Zhang, J. Alloys Compd. 494 (2010) 330–335.
[6] J.H. Shen, Y. Bai, J. Zhou, L.T. Li, J. Am. Ceram. Soc. 88 (2005) 3440–3443.
[7] L.J. Jia, S.C. Chen, H.W. Zhang, Z.Y. Zhong, Mater. Chem. Phys. 114 (2009) 697–701.
[8] A.S. Fawzi, A.D. Sheikh, V.L. Mathe, J. Alloys Compd. 493 (2010) 601–608.
[9] M.A. Subramanian, D. Li, N. Duan, B.A. Reisner, A.W. Sleight, J. Solid State Chem. 151 (2000) 323–325.
[10] A.P. Ramirez, M.A. Subramanian, M. Gardel, G. Blumberg, D. Li, T. Vogt, S.M. Shapiro, Solid State Commun. 115 (2000) 217–220.
[11] Y. He, H.W. Zhang, W.W. Ling, C.H. Mu, Y.X. Li, J. Shen, IEEE Trans. Magn. 45 (2009) 4314–4316.
[12] J. Muller, H. Thust, K.H. Drue, Int. J. Microcircuits Electron. Packaging 18 (1995) 200–206.
[13] J.J. Liu, R.W. Smith, W.N. Mei, Chem. Mater. 19 (2007) 6020–6024.
[14] B.P. Zhu, Z.Y. Wang, Y. Zhang, Z.S. Yu, J. Shi, R. Xiong, Mater. Chem. Phys. 113 (2009) 746–748.
[15] S.D. Hutagalung, L.Y. Ooi, Z.A. Ahmad, J. Alloys Compd. 476 (2009) 477–481.
[16] H. Su, H.W. Zhang, X.L. Tang, Mater. Sci. Eng. B 117 (2005) 231–234.
[17] M. Drofenik, A. Znidarsic, D. Makovec, J. Am. Ceram. Soc. 81 (1998) 2841–2848.
[18] J.L. Snoek, Physica 14 (1948) 207–217.
[19] H. Su, H.W. Zhang, X.L. Tang, Y. Shi, J. Magn. Magn. Mater. 320 (2008) 483–485.
[20] M.T. Johnson, E.G. Visser, IEEE Trans. Magn. 26 (1990) 1987–1989.
[21] L.B. Kong, M.L.S. Teo, Z.W. Li, G.Q. Lin, Y.B. Gan, J. Alloys Compd. 459 (2008) 576–582.
[22] T. Nakamura, T. Tsutaoka, K. Hatakeyama, J. Magn. Magn. Mater. 138 (1994) 319–328.
[23] L.B. Kong, Z.W. Li, G.Q. Lin, Y.B. Gan, Acta Mater. 55 (2007) 6561–6572.
[24] N. Rezlescu, E. Rezlescu, Phys. Status Solidi A 23 (1974) 575–582.
[25] W.D. Kingery, H.K. Bowen, D.R. Uhlmann, Introduction to Ceramics, John Wiley, New York, 1976, pp. 913–945.
[26] Z. Yu, C. Ang, J. Appl. Phys. 91 (2002) 794–797.